Atmospheric Research 281 (2023) 106494

Contents lists available at ScienceDirect

Atmospheric Research

journal homepage: www.elsevier.com/locate/atmosres

Historical evaluation and projection of precipitation phase changes in the cold season over the Tibetan Plateau based on CMIP6 multimodels

Guodong Wang [a], Yongli He [a,b,*], Boyuan Zhang [a], Xiaoxia Wang [a], Shanjun Cheng [c], Yongkun Xie [b], Shanshan Wang [a], Xiaodan Guan [a,b]

[a] Key Laboratory for Semi-Arid Climate Change of the Ministry of Education, College of Atmospheric Sciences, Lanzhou University, Lanzhou, Gansu, China
[b] Collaborative Innovation Center for Western Ecological Safety, Lanzhou, China
[c] Tianjin Climate Center, Tianjin 300074, China

ARTICLE INFO

Keywords:
Enhanced warming in the cold season
CMIP6
Precipitation phase
Tibetan Plateau

ABSTRACT

The solid precipitation in the cold season over the TP is important for the recharge of snow cover, glaciers, rivers, etc. During the past decades, the TP has experienced enhanced warming in the cold season, which could transfer more snowfall to rainfall and influence the land-atmosphere hydrological cycle of the Asian water tower. However, most CMIP6 models underestimate the cold season temperature and overestimate the total precipitation, and the performance of the precipitation phase in the CMIP6 simulations remains unclear. This study investigates the precipitation phase bias in the cold season by comparing simulations from CMIP6 to observations. The results suggest that the snowfall-to-precipitation ratio (SPR) from CMIP6 was significantly underestimated, and the SPR at the southern edge of the TP was underestimated by approximately 30%. However, the decreasing trend of SPR is significantly overestimated. Comparing the influence of the surface temperature and total precipitation, the correlation coefficient between the mean SPR bias and the simulated temperature bias is −0.701 with a 99% confidence level, which is much greater than that with total precipitation bias. The mean SPR in the seven best models is much greater than the ensemble mean of the original 23 CMIP6 models over the TP. Moreover, the SPR varies significantly under different future scenarios. Under the most severe scenario, the decrease in SPR exceeds −21.45%, substantially influencing the water balance over the TP, while the decline is only −9.79% under the weak scenario. Therefore, the warming caused by high emissions should not be ignored when projecting the precipitation phase, and the significant effect of surface temperature on the precipitation phase requires additional consideration when investigating the hydrological cycle imbalance over the TP.

1. Introduction

Located in the mid-latitudes of the Asian continent, the Tibetan Plateau (TP) is the highest plateau in the world, with an average elevation of >4000 m (Kang et al., 2010; Yao et al., 2012). The TP has complex terrain and abundant water resources, and it is the birthplace of 12 important rivers in Asia, including the Yangtze, Yellow, Indus, Brahmaputra, and Ganges Rivers. Due to its huge water storage, the TP has an important impact on the downstream economic society, where it has billions of people; therefore, the TP is also called the "Asian water tower" (Lu et al., 2005; Xu et al., 2008; Immerzeel and Bierkens, 2012). As the Earth's recognized "Third Pole", the TP has a considerable influence on the regional hydrological cycle and even global climate through thermal and dynamic effects (Allen and Ingram, 2002; Xu et al., 2014; Yao et al., 2019). Under global warming, the climate over the TP has changed significantly (Yao et al., 2012; Duan and Xiao, 2015; He et al., 2021). Therefore, it is of great significance to study climate changes on the TP.

As one of the most sensitive regions to global warming, the TP is experiencing the most enhanced climate changes (Immerzeel et al., 2010; Yao et al., 2019; Huang et al., 2019). The warming rate of surface temperature over the TP has been nearly twice as fast as the global mean warming rate in recent decades, especially during the cold season (Rangwala et al., 2009; Chen et al., 2015; Kuang and Jiao, 2016). Under the influence of enhanced warming, the total column of water vapor and precipitation has significantly increased (Sun et al., 2020; He et al.,

* Corresponding author at: Key Laboratory for Semi-Arid Climate Change of the Ministry of Education, College of Atmospheric Sciences, Lanzhou University, Lanzhou, Gansu, China.
E-mail address: heyongli@lzu.edu.cn (Y. He).

https://doi.org/10.1016/j.atmosres.2022.106494
Received 14 June 2022; Received in revised form 3 September 2022; Accepted 26 October 2022
Available online 29 October 2022

2021) and is projected to continually increase in the future (Yang et al., 2021; Zhao et al., 2022). However, the increasing precipitation may not compensate for the decreasing terrestrial water storage (TWS) associated with the melting of solid water (glaciers, permafrost, snow cover, etc.), which may be related to the precipitation phase. A recent study found that surface warming could change the vertical profile of temperature and increase the atmospheric melting level height, which could facilitate the conversion of snowfall to rainfall (Prein and Heymsfield, 2020). Rainfall would quickly flow out of the TP through runoff due to its short local residence times (Wang et al., 2022). Therefore, the precipitation phase associated with rainfall and snowfall is important for the hydrological cycle. However, few studies have investigated the precipitation phase changes over the TP, especially in the cold season, which greatly impacts terrestrial water storage (Wang et al., 2022). Local water balance and ecological balance are further threatened (Chen et al., 2015; Meng et al., 2019; Yao et al., 2019). With global warming, the decrease in solid precipitation and the increase in liquid precipitation will lead to the movement of the freezing precipitation belt, which will endanger the electrical transmission network and distribution infrastructure (Tropea and Stewart, 2021). In the TP area with dense hydropower stations, the loss caused by freezing precipitation may be greater. Therefore, it is important to study the precipitation phase changes in the cold season over the TP, which lays a foundation for accurately predicting future precipitation and taking countermeasures.

The Coupled Model Intercomparison Project Phase 6 (CMIP6) contains the latest and advanced climate models developed by research institutes in different countries around the world, which provides a new perspective for investigating the precipitation change over the TP (Eyring et al., 2016; Zhao et al., 2022). CMIP6 models simulate long-term historical climate and make projections based on future scenarios, which is widely employed to study climate change (McCrystall et al., 2021; Wang et al., 2021; Zhu et al., 2021). Using CMIP6 to study the TP regional climate has gradually attracted more attention (Li et al., 2021; Peng et al., 2022). However, the applicability of each CMIP6 model varies in different climate regions (Rivera and Arnould, 2020; Yazdandoost et al., 2021; Li et al., 2021); therefore, it is necessary to evaluate the performance of the CMIP6 models on the TP. Because few previous studies have investigated precipitation phase changes over the TP, the simulation ability of precipitation phase changes in CMIP6 models is still unclear.

Previous studies associated with the evaluation of temperature and precipitation over the TP have shown a temperature “cold bias” over the TP by CMIP6 simulated data; that is, the temperature simulated by the model is generally lower than the actual temperature (Su et al., 2013; Chen et al., 2017; Lun et al., 2021), especially in winter (Jia et al., 2019; Peng et al., 2022). The cold bias of surface temperature may influence the vertical temperature profile and the melting level height, which is a key factor for precipitation phase changes. However, whether the cold bias has an influence on the bias of the precipitation phase remains unclear. Therefore, it is of practical significance to evaluate the performance of CMIP6 models in simulating precipitation phases over the TP, which helps analyze the characteristics of different precipitation phases and, further, establish an accurate prediction model for future precipitation over the TP.

This study aims to (1) evaluate the performance of CMIP6 models in simulating the precipitation phase in the cold season over the TP, (2) explore the reasons for the precipitation phase bias between CMIP6 models and observed data, and (3) provide SPR projections under different scenarios in the future. Answering the above questions will provide a scientific reference for future precipitation change projections and model improvement. The rest of this study is arranged as follows. Section 2 describes the data and methodology used in this study, including the method of dividing rainfall and snowfall from total precipitation. Section 3 evaluates the performance of 23 CMIP6 models in simulating the climatology and trend of the precipitation phase in the cold season over the TP, discusses the linkage between temperature bias and precipitation phase bias between models, and then selects a group of models with good historical simulation ability to give preliminary future projections under different scenarios. Section 4 discusses the possible mechanisms of precipitation phase bias in CMIP6 models and their implications and finally summarizes this study.

2. Data and methodology

2.1. Observation data

The observation data used in this study are the China Meteorological Forcing Dataset (CMFD), which has a high spatial resolution of 0.1° × 0.1° and covers 1979 to 2018 (http://data.tpdc.ac.cn/en/data/8028b944-daaa-4511-8769-965612652c49/). It is the first dataset that integrates remote sensing products, reanalysis datasets, and in situ station data to study land surface processes in China (Yang and He, 2019; He et al., 2020). Due to the good temporal and spatial uniformity of the CMFD, it has been widely used to study climate issues, especially in the TP region (Nury et al., 2019; Lun et al., 2021; Peng et al., 2022). To analyze the change in the precipitation phase in recent decades and evaluate the simulation ability of CMIP6, we used the 3-hourly average surface air temperature and total precipitation. Snowfall and rainfall in the cold season (defined as the period from October to April) were separated from total precipitation by a dynamic threshold parameterization scheme (Ding et al., 2014), which used CMFD 3-hourly average specific humidity, pressure, etc.

2.2. Satellite data

The Global Precipitation Measurement (GPM) mission is a satellite network observation system initiated by the National Aeronautics and Space Administration (NASA) and Japan Aerospace Exploration Agency (Japan Aerospace Exploration Agency), obtaining global precipitation data through the Dual-Frequency Precipitation Radar (DPR) and GPM Microwave Imager (GMI) (Hou et al., 2014). The Integrated Multi-satellitE Retrievals for GPM (IMERG) algorithm is based on the precipitation observational information from the above GPM detectors and combined with the data from the Tropical Rainfall Measuring Mission (TRMM) as much as possible (Li et al., 2022). The latest version (V06) of the IMERG final run product (Huffman et al., 2019) is used in this study, with a spatial resolution of 0.1° × 0.1° and a time resolution of 30 min. Previous studies have shown that IMERG datasets have good applicability in the TP region (Li et al., 2020; Li et al., 2022). However, the IMERG dataset has been recorded since June 2000; it only has data from nearly two decades, so IMERG was regarded as the verification of the CMFD results in this study.

2.3. Model data

Monthly surface air temperature, precipitation, and snowfall were obtained from 23 CMIP6 models (https://esgf-node.llnl.gov/search/cmip6/). Table 1 provides a detailed description of each model. Note that the historical simulations of CMIP6 are 1850–2014, and future climate projections SSP2–4.5/SSP5–8.5 cover the period 2015–2100 (O’Neill et al., 2016; Gidden et al., 2019). SSP2–4.5 represent the closest to the current emission scenarios, and SSP5–8.5 represent the high emission scenarios. To match the CMFD (1979–2018), we merged historical simulations (1979–2014) with SSP2–4.5 future projections (2015–2018) as the historical period in this study. Before our calculation, each CMIP6 model’s data were regridded via the bilinear interpolation method to 1.25° × 1.25° grids, ensuring the resolution uniformity between different models. The ground observation and satellite data were also processed similarly before being compared and evaluated.

Table 1
List of Coupled Model Intercomparison Project Phase 6 (CMIP6) models used in this study.

No.	CMIP6 models	Institution	Horizontal Resolution (latitude × longitude)
1	ACCESS-CM2	Commonwealth Scientific and Industrial Research Organization (Australia)	1.25° × 1.875°
2	ACCESS-ESM1–5	Commonwealth Scientific and Industrial Research Organization (Australia)	1.25° × 1.875°
3	BCC-CSM2-MR	Beijing Climate Center, China Meteorological Administration (China)	1.1215° × 1.125°
4	CMCC-CM2-SR5	Fondazione Centro Euro-Mediterraneo sui Cambiamenti Climatici (Italy)	0.9424° × 1.25°
5	EC-Earth3	EC-Earth-Consortium (Europe)	0.70° × 0.70°
6	EC-Earth3-CC	EC-Earth-Consortium (Europe)	0.70° × 0.70°
7	EC-Earth3-Veg	EC-Earth-Consortium (Europe)	0.70° × 0.70°
8	EC-Earth3-Veg-LR	EC-Earth-Consortium (Europe)	1.1215° × 1.125°
9	FGOALS-g3	Institute of Atmospheric Physics, Chinese Academy of Sciences (China)	2.0253° × 2°
10	FIO-ESM-2-0	The First Institution of Oceanography (China)	0.9424° × 1.25°
11	GFDL-ESM4	Geophysical Fluid Dynamics Laboratory, Princeton (USA)	1° × 1.25°
12	INM-CM4–8	Institute for Numerical Mathematics, Russian Academy of Science (Russia)	1.5° × 2°
13	INM-CM5–0	Institute for Numerical Mathematics, Russian Academy of Science (Russia)	1.5° × 2°
14	IPSL-CM6A-LR	Institut Pierre Simon Laplace (France)	1.2676° × 2.5°
15	KACE-1-0-G	National Institute of Meteorological Sciences/Korea Meteorological Administration (Republic of Korea)	1.25° × 1.875°
16	MIROC6	Agency for Marine-Earth Science and Technology (Japan)	1.4008° × 1.406°
17	MPI-ESM1–2-HR	Max Planck Institute for Meteorology (Germany)	0.935° × 0.9375°
18	MPI-ESM1–2-LR	Max Planck Institute for Meteorology (Germany)	1.865° × 1.875°
19	MRI-ESM2–0	Agency for Marine-Earth Science and Technology (Japan)	1.1215° × 1.125°
20	NESM3	Nanjing University of Information Science and Technology (China)	1.865° × 1.875°
21	NorESM2-LM	Norwegian Climate Centre (Norway)	1.895° × 2.5°
22	NorESM2-MM	Norwegian Climate Centre (Norway)	0.9424° × 1.25°
23	TaiESM1	Research Center for Environmental Changes, Academia Sinica, Taipei (China)	0.9424° × 1.25°

2.4. Statistical metrics

To evaluate the ability of each CMIP6 model to reproduce the observed data in the cold season over the TP, several statistical metrics were calculated based on the time scale or spatial scale, including the mean bias error (MBE), pattern correlation coefficient (PCC, e.g., Shiferaw et al., 2018; Rivera and Arnould, 2020), root-mean-square error (RMSE, e.g., Duan et al., 2016), trend, and interannual variability skill score (IVS, e.g., Scherrer, 2011; Peng et al.,2022). Their values are calculated by Eqs. (1)–(4).

$$\mathrm{MBE} = \frac{\sum_{i=1}^{N}(y_i - o_i)}{N} \tag{1}$$

$$\mathrm{RMSE} = \sqrt{\frac{\sum_{i=1}^{N}(y_i - o_i)^2}{N}} \tag{2}$$

where y_i and o_i are the CMIP6 simulated and observed data at the ith grid point. N is the total number of grid points. The closer their values are to 0, the better the simulation.

$$\mathrm{PCC} = \frac{\sum_{i=1}^{N}(y_i - \overline{y})(o_i - \overline{o})}{\left(\sum_{i=1}^{N}(y_i - \overline{y})^2 \sum_{i=1}^{N}(o_i - \overline{o})^2\right)^{\frac{1}{2}}} \tag{3}$$

where $\overline{y}$ and $\overline{o}$ refer to the mean values of CMIP6 simulated and observed data over the N grid points, respectively. The PCC ranges from −1 to 1, with values closer to 1 indicating a greater ability of the models to capture the spatial patterns of the observed data over the region.

$$\mathrm{IVS} = \left(\frac{STD_i}{STD_o} - \frac{STD_o}{STD_i}\right)^2 \tag{4}$$

where STD_i and STD_o represent the standard deviations of the simulation and observation, respectively. It should be mentioned that we first calculate the values at each grid point and then average them over the TP. The smaller the IVS score is, the better the simulation.

2.5. Dynamic Threshold Parameterization Scheme

Before evaluating the performance of CMIP6 models in simulating the precipitation phase in the cold season over the TP, the precipitation in CMFD must be separated into rainfall and snowfall. This study uses the estimated snowfall determined by the dynamic threshold parameterization scheme (DTPS), an empirical method to distinguish precipitation types through surface air conditions (Ding et al., 2014). DTPS has been demonstrated to capture snowfall changes well over the TP through comparison with station observations (Ding et al., 2014). The precipitation type is determined by

$$type = \begin{cases} snow, T_w \le T_{min} \\ sleet, T_{min} < T_w < T_{max} \\ rain, T_w \ge T_{max} \end{cases} \tag{5}$$

where T_w is the surface wet-bulb temperature, which is more useful than the surface dry-bulb temperature because it considers evaporative cooling effects (Bocchieri, 1980; Tamang et al., 2020). The two threshold temperatures (T_{min} and T_{max}) are obtained by elevation (Z) and 3-hourly near-surface specific humidity (RH) data from CMFD. For more details of T_{min} and T_{max}, the reader should refer to Ding et al. (2014). Notably, in addition to considering the physical process of snowfall melting, the DTPS also focuses on elevation and surface meteorological conditions to retain dynamical threshold temperatures on each grid. As an effective method to distinguish precipitation types over the TP, the DTPS has been widely used in many studies (Deng et al., 2017; Luo et al., 2020; Yang et al., 2021; Wang et al., 2022). A previous study demonstrated that the probability of sleeting over the TP is less than that of rain and snow (Ding et al., 2014). To enable follow-up work, we classified half of the sleet as rainfall and the other half as snowfall.

3. Result

3.1. The bias in the climatology of temperature and precipitation in the cold season

Due to the complex terrain over the TP, most climate models have a relatively worse performance for temperature and precipitation in this region than the global mean (Su et al., 2013; Chen and Frauenfeld, 2014; Palazzi et al., 2015; Lun et al., 2021). To evaluate the performance of the precipitation phase in the CMIP6 models, the bias of climatology of temperature and precipitation in the cold season was first investigated (Figs. 1 and 2). The result suggests a “cold bias” in the cold season (October to April) over the TP. In most areas of the TP, the observed

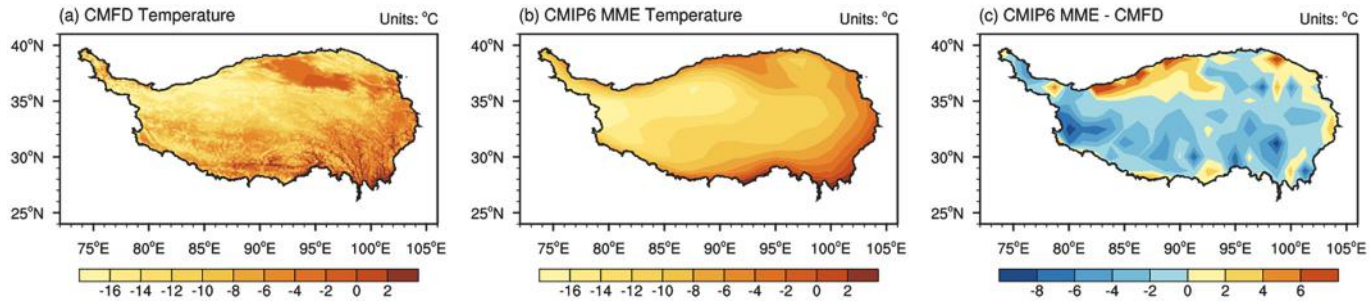

Fig. 1. The spatial distribution of the cold-season average temperature based on (a) CMFD and (b) CMIP6 MME during 1979–2017; (c) the bias between CMFD and CMIP6 MME during 1979–2017.

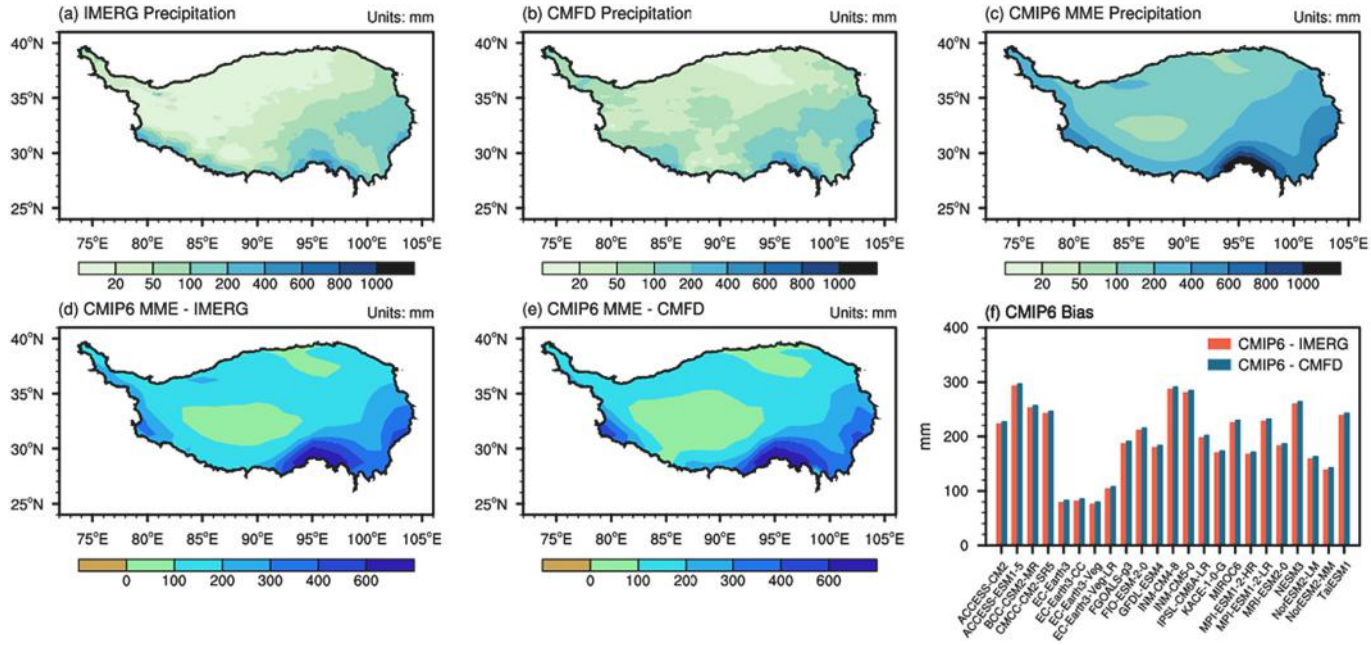

Fig. 2. The spatial distribution of the cold-season average cumulative precipitation based on (a) IMERG, (b) CMFD and (c) CMIP6 MME during 2000–2017. The bias between CMIP6 MME and (d) IMERG, (e) CMFD during 2000–2017. (f) The bias between 23 CMIP6 models and two kinds of observed data.

climatological mean temperature in the cold season was lower than 0 °C, and the lowest temperature in the northwest of the TP was below −16 °C (Fig. 1a). The multimodel ensemble mean (MME) results of 23 CMIP6 models show a consistent spatial distribution with the observed data. The temperature decreased from the southeast to the northwest, with higher temperatures at the eastern, southern, and northern edges of the TP. However, the lowest temperature occurred more westward, making the temperature change smoother (Fig. 1b). Except for a few marginal areas in the northern and eastern TP, the climatological mean temperature in the cold season simulated by the models was relatively low. In the southwestern TP, the MME result of all 23 models was even 8° lower than the observations, which was larger than the "cold bias" in the cold-season mean temperature (Fig. 1c). Such a large "cold bias" may significantly affect atmospheric melting level height (Wang et al., 2022), but the impact on the precipitation phase remains unclear.

Based on CMFD, IMERG observed data, and CMIP6 simulated data, the climatological cumulative precipitation in the cold season over the TP during the 2000–2017 period is shown in Fig. 2. The precipitation from CMFD and IMERG are consistent, indicating that the observational results have been verified by each other. The spatial distribution of precipitation is highly uneven, decreasing from southeast to northwest, with a fluctuation of approximately 600 mm. The maximum precipitation is nearly located on the southern edge of the longitude 95°E (Fig. 2a–b). The CMIP6 MME can capture the spatial distribution of precipitation decreasing from southeast to northwest and the location of the precipitation maximum value, but the area of the precipitation minimum value is biased (Fig. 2c). Moreover, the precipitation of CMIP6 MME is generally overestimated, and the precipitation is even overestimated by 2–3 times in the southern TP (Fig. 2d–e). Fig. 2f shows the bias between each CMIP6 model and two kinds of observed data. There are great differences between models. The bias of the EC-Earth3-Veg model with the best performance is approximately 80 mm, and the bias of ACCESS-ESM1–5 with the worst performance is nearly 300 mm. The wetting bias is related to the overestimated wind speed and humidity caused by the reduced terrain dragging effect in the coarse resolution of climate models (Wang et al., 2020). However, whether the large uncertainty of total precipitation influences the simulation of the precipitation phase remains unknown.

3.2. *Evaluation of the simulated precipitation phase*

3.2.1. *The climatology of the precipitation phase in the cold season*

In recent years, the proportion of snowfall or rainfall in the total precipitation has gradually received increasing attention from the scientific community (Wang et al., 2016; Deng et al., 2017; Prein and Heymsfield, 2020). The snowfall-to-precipitation ratio (SPR) is a widely

used index representing the precipitation phase (Tamang et al., 2020; McCrystall et al., 2021). The range of SPR is between 0 and 1. The larger the SPR is, the more snowfall there is relative to rainfall. We use the CMFD as the reference to evaluate the simulation ability of the precipitation phase in CMIP6 during the 1979–2017 period. Fig. 3a-c shows the spatial distribution of the climatology of snowfall, rainfall, and SPR from the CMFD in the cold season. During this period, total precipitation is dominated by snowfall over the TP; SPR is even >95% in the central and western TP (Fig. 3c). The rainfall is concentrated in the southeastern region of the TP. In contrast, the snowfall is much larger, >240 mm, in the southern region of the TP (Fig. 3b). Fig. 3d-f shows the spatial distribution of the climatology of snowfall, rainfall, and SPR based on the CMIP6 MME result. They can capture the spatial distribution of snowfall, rainfall, and SPR over the TP. However, there is more snowfall and rainfall in the CMIP6 MME, and the areas with snowfall exceeding 240 mm and rainfall exceeding 200 mm are significantly expanded (Fig. 3d-e). The changes in their magnitude lead to a decrease in the SPR, so the area with an SPR exceeding 95% shrinks to the west (Fig. 3f). Fig. 3g–i shows the spatial distribution of the biases of snowfall, rainfall, and SPR between the CMIP6 MME and CMFD. The results suggest that the SPR is underestimated in CMIP6, although snowfall and rainfall are overestimated over the TP, especially in the southern TP (Fig. 3g and h).

Furthermore, to investigate the performance of the individual models, Fig. 4 shows the biases of snowfall, rainfall, and SPR in each model. The result suggests that the overestimation of snowfall and rainfall occurred in all models. The CMIP6 MME results show that the overestimation of snowfall is close to 150 mm (Fig. 4a), and the overestimation of rainfall is >40 mm (Fig. 4b). Most models underestimate SPR in the cold season over the TP, but there are great differences in SPR bias between different models from −16.75% to 7.01% with a mean of −3.27% (Fig. 4c). Model resolution may affect the underestimation of the SPR. Low-resolution data in CMIP6 cannot accurately characterize the complex terrain of the TP and only reflect flatter terrain. Weak orographic drag and strong water vapor transport lead to an overestimation of total precipitation. When total precipitation is overestimated, rainfall is overestimated more than snowfall (Fig. 6b). In addition, the DTPS is sensitive to the surface temperature, which has a large uncertainty in the CMIP6 low-resolution data due to the absence of the effect of complex terrain.

From the above analysis of the CMIP6 models in historical SPR simulations, it can be concluded that CMIP6 MME results still have deficiencies in reproducing the climatology and spatiotemporal variability of SPR in the cold season over the TP. Therefore, it is necessary to analyze the performance of each model. Based on the SPR scores by PCC, IVS, Trend and RMSE, we evaluated the performance of 23 CMIP6 models in reproducing the SPR in the cold season over the TP during the 1979–2017 period. Their score details are given in supplementary Table S1, and we calculated the four metrics for each model to obtain the individual ranking of each model. A lower ranking number in Fig. 5 indicates better performance of the individual model. The final ranking of each CMIP6 model is shown in the rightmost column of Fig. 5, which is determined by the average of the ranks in the left four columns of Fig. 5 based on the above metrics. The top model means that it has a good ability to reproduce the SPR both in spatial distribution and temporal changes, while the bottom model means that it has a poor ability, such as NorESM2-LM. Hence, the top 30% of models are adopted as a group of models with good performance in reproducing the SPR in the cold season over the TP. The top seven models are EC-Earth3-Veg, MPI-

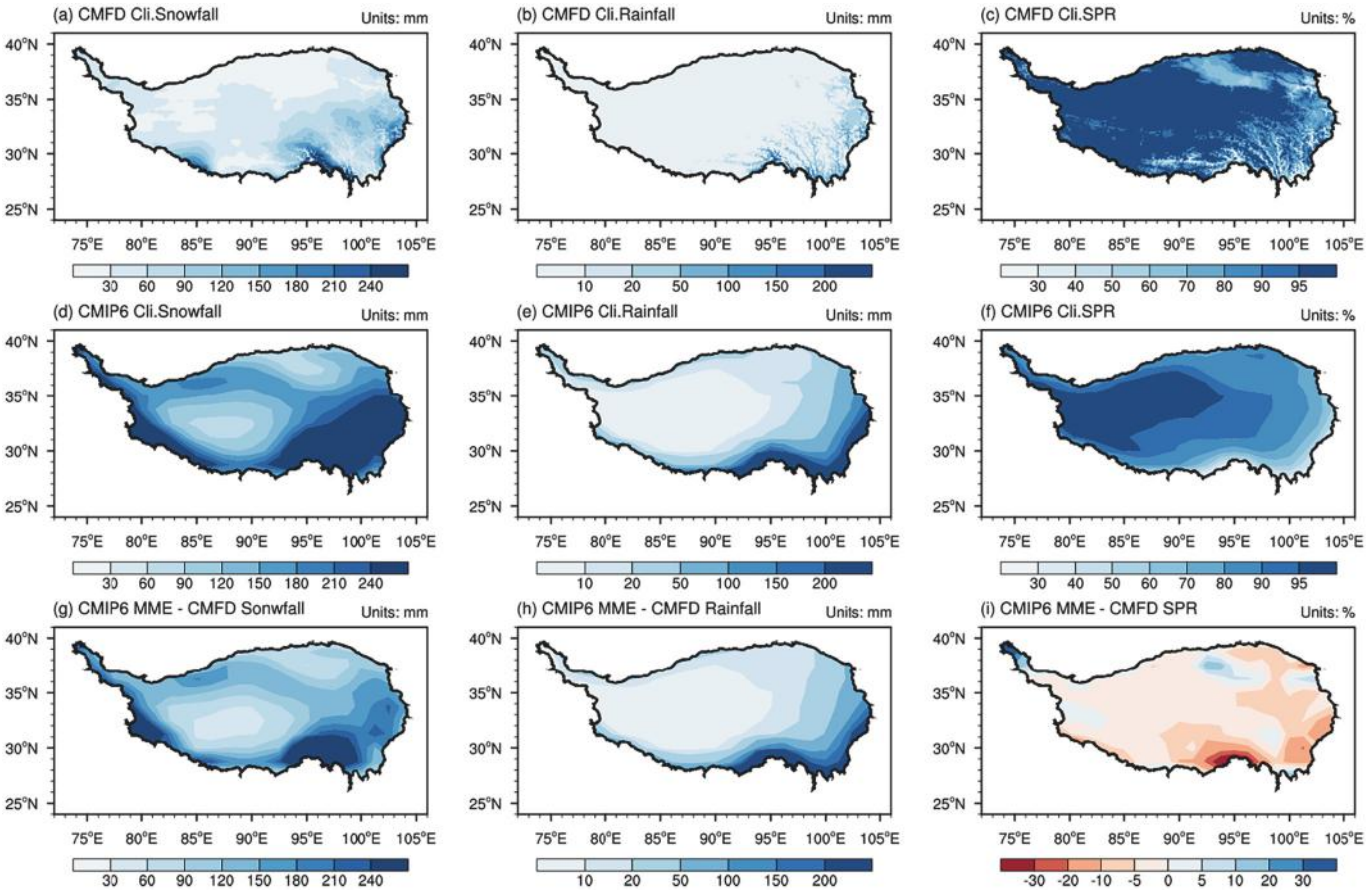

Fig. 3. The spatial distribution of the climatology of (a) cumulative snowfall, (b) cumulative rainfall and (c) average SPR in the cold season from CMFD during 1979–2017. (d) - (f) are the same as (a) - (c) but for CMIP6 MME. The spatial difference in the cold-season average (g) cumulative snowfall, (h) cumulative rainfall and (i) SPR between CMIP6 MME and CMFD during 1979–2017.

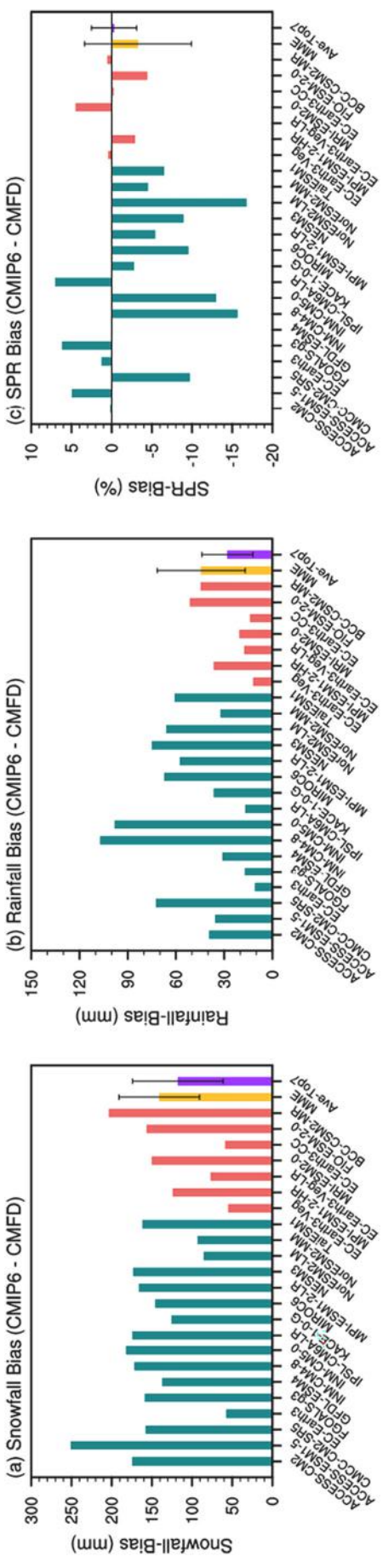

Fig. 4. Cold season average (a) snowfall bias, (b) rainfall bias and (c) SPR bias over the TP during the 1979–2017 period. The red bars represent the seven best models for SPR simulation, the green bars represent other models, the yellow bar represents CMIP6 MME, and the purple bar represents MME of the seven best models. The error bar denotes the two standard deviations of simulations. (For interpretation of the references to colour in this figure legend, the reader is referred to the web version of this article.)

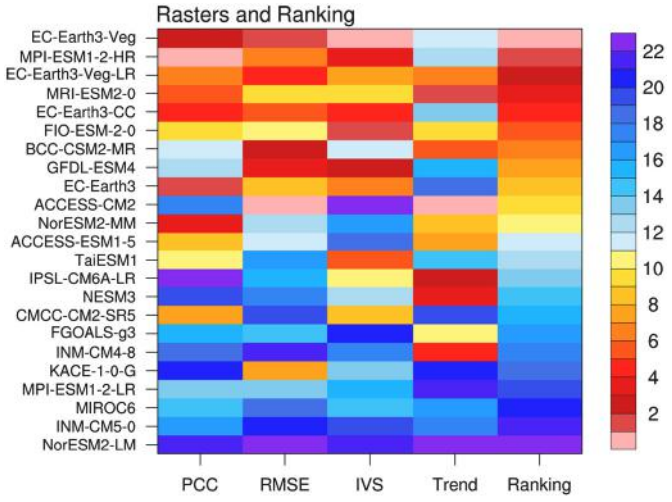

Fig. 5. Rankings of the 23 CMIP6 models in reproducing the cold-season average SPR over the TP during the 1979–2017 period. The better the simulation, the lower the ranking number. The metrics from left to right represent the rankings of the PCC, RMSE, IVS, trend score and overall ranking.

ESM1–2-HR, EC-Earth3-Veg-LR, MRI-ESM2–0, EC-Earth3-CC, FIO-ESM-2-0, and BCC-CSM2-MR. For the seven best models of SPR simulation, the biases of snowfall, rainfall, and SPR are much smaller than those of the other models (Fig. 4c).

3.2.2. *The trend of the precipitation phase in the cold season*

To investigate the temporal variation in the precipitation phase, the time series of snowfall and rainfall anomalies in the cold season were first investigated based on the CMFD and CMIP6 MME datasets, as shown in Fig. 6a. Due to the large bias of the climatology of snowfall and rainfall, the anomaly was used to investigate the temporal variation. During the past four decades, the observed rainfall shows a larger interannual variability and increasing trend than snowfall. The rainfall and snowfall from CMIP6 MME have a weaker interannual variability than CMFD, and there is an increasing trend of rainfall, but there is no significant snowfall trend. Therefore, the SPR would decrease, indicating that the proportion of snowfall in the total precipitation would decrease, as shown in Fig. 6b. The results suggest that the observed SPR from the CMFD dataset has decreased by −0.153%/decade in the past four decades, with a large interannual fluctuation. The simulated SPR from the CMIP6 MME is −0.88%/decade, much faster than that of the CMFD dataset.

It is noted that the trend of snowfall for each model is diverse, and the trend of rainfall is consistently increasing except for the GFDL-ESM4 model, which demonstrates that the uncertainty of simulated snowfall is larger than that of rainfall (Fig. 7a and b). However, except for GFDL-ESM4, the trend of the simulated SPR in each model is negative bias, which means that the simulated SPR by CMIP6 decreased faster than the observed data. The mean SPR trend is greater than the MME trend for the seven best models and passes the significance test ($p < 0.05$) (Fig. 7c). Although the observed trend in SPR is not statistically significant, the SPR trend predicted by the seven best models is closer to the observation than that predicted by MME. It has been proven that selecting a group of models with good simulation ability is conducive to reducing the bias, which is of practical significance to the application of climate models.

In general, the simulated rainfall and snowfall in the CMIP6 models are both larger than those in the CMFD in the cold season over the TP during the 1979–2017 period, but the SPR simulated by most models is smaller than the observed value. Meanwhile, the seven best models of SPR in the cold season have less rainfall bias and snowfall bias than the CMIP6 MME. Although the climatology of rainfall and snowfall from the

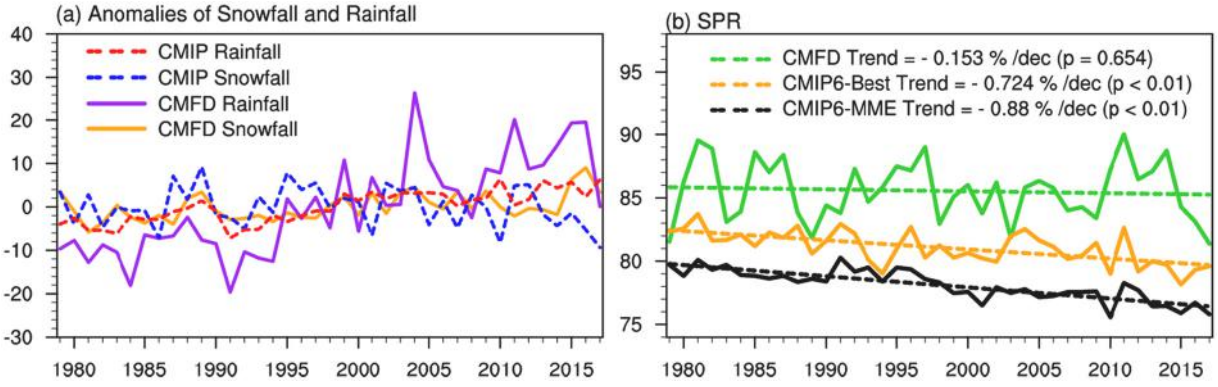

Fig. 6. (a) Time series of rainfall and snowfall anomalies in the cold season over the TP during the 1979–2017 period. (b) Time series of SPR in the cold season over the TP during the 1979–2017 period.

CMIP6 models is overestimated, the mean SPR in the cold season is underestimated, and the trend of SPR is overestimated.

3.3. Possible mechanism of precipitation phase bias in CMIP6 models

Due to the influence of the precipitation phase on the recharge of surface solid water, understanding the mechanism of precipitation phase bias is important for improving the performance of model simulations. The precipitation phase bias over the TP may be caused by the bias of the local climate physical quantities. In other words, the SPR bias is related to the bias in the thermal process (vertical temperature profile) and dynamic progress (precipitation) between CMIP6 models and the observation. The cold bias of surface temperature may induce the bias of the vertical temperature profile. To explore the mechanism of the SPR bias in the cold season over the TP during the 1979–2017 period, the relationship between the average SPR bias and the average temperature bias/precipitation bias was investigated (Fig. 8). Most models show "cold bias and negative SPR bias", which is consistent with the CMIP6 MME results. According to the simulation results of different models, as the temperature bias changes from negative to positive, the SPR bias gradually changes from positive to negative in the cold season over the TP, and the correlation coefficient between them reaches −0.701, with a 99% confidence level (Fig. 8a). However, the correlation coefficient between the SPR bias and the total precipitation bias in the cold season is only −0.333, which does not pass the 90% significance test. The result suggests that both the temperature "cold bias" and precipitation "wet bias" of the model contribute to the bias of SPR in the cold season, but the SPR is more sensitive to changes in temperature and not to precipitation. Therefore, the cold bias is a very important reason for the SPR bias in the cold season over the TP in the CMIP6 models, and the models with lower surface temperatures tend to show higher SPRs. However, negative SPR bias also exists in some models when the cold bias falls between −4 and 0°, which suggests that other mechanisms also influence the precipitation phase over the TP simulated by CMIP6 models, such as total precipitation bias and atmospheric moisture bias in the cold season.

To verify the influence of surface temperature on the SPR, we further investigated the relationship between the surface temperature- trend and the SPR- trend in the cold season over the TP during the 1979–2017 period (Fig. 9). The result suggests that the correlation coefficient reached −0.51 with a 95% confidence level. Using the bootstrapped cross-correlation method (Gilleland, 2020), we confirmed the negative correlation between them once more. The average bootstrapped cross-correlation coefficient calculated by 1000 experiments also reached −0.5 (−0.79 ~ −0.04) with a 90% confidence level (Fig. S1). This means that the rising rate of temperature between models is larger, and the decreasing trend of snowfall percentage is also significantly larger. The lack of significance of the decreasing trend of cold-season SPR in CMFD compared to CMIP6 (Fig. 6b) may be due to the higher increasing trend of surface temperature in CMIP6. In addition, the significant trend of cold-season SPR in the CMIP6 models is impacted by additional factors, such as overestimated water vapor transportation due to low-resolution topography and the bias of SPR induced by the cloud physical parameterization scheme.

3.4. The projected changes in the precipitation phase in the future

Based on the ranking of model performance of the precipitation phase, the top seven best models were chosen to make the projection of precipitation phase change in the future to reduce the uncertainty. Before that, we investigated the bias of the seven best models in the cold season compared with that in the MME from all models. The results show that the difference in SPR between the seven best models and CMFD is relatively small (Fig. 10a) compared with the difference between 23 CMIP6 models and CMFD (Fig. 3i). For the result simulated by the seven best models, the bias is less than −5% in most areas of the TP, except the northwest edge and the Brahmaputra basins (Fig. 10a). In most areas of the TP, the SPR is larger than that simulated by the 23 CMIP6 models and is more significant in the southern areas, where the SPR bias even increased by >10% (Fig. 10b). This result suggests that although the cold-season SPR simulated by the seven best models is also underestimated, it has a large improvement over the MME of 23 models, especially in the southern TP. Therefore, the top seven best models have great potential for making future projections.

Fig. 11 shows the historical and projected SPR in the cold season over the TP during the 1979–2099 period from the seven best models. The results suggest that compared with the historical period (1979–2013), the SPR will decline rapidly in the next few decades under different scenarios. In the SSP245 scenario, which is closer to the current situation, the decline rate of SPR will be −1.17%/dec in the future, while in the high emission scenario SSP585, the decline rate of SPR will reach −2.88%/dec (Fig. 11a). The above results all pass the significance test at the 99% confidence level. The projected changes in SPR in the cold season during the near-term (2020–2039), mid-term (2040–2059), and long-term (2080–2099) are further compared. In the near-term future, the SPR changes under the middle and high emission scenarios have little difference, with average decreases of −2.93% and −3.38%, respectively. In the mid-term future, the SPR of the two scenarios has been significantly different, with average decreases of −5.13% and −7.2%, respectively. In the long term, the difference is considerable, and the SPR will decrease by −9.79/−21.45% in SSP245/SSP585. The accelerated decline in SPR in the cold season is consistent with the projected intensified warming over the TP in the future (Peng et al.,2022), indicating that accelerated warming will have a significant impact on the local precipitation phase changes in the cold season over the TP. In the worst scenario, the SPR in the cold season will decrease by

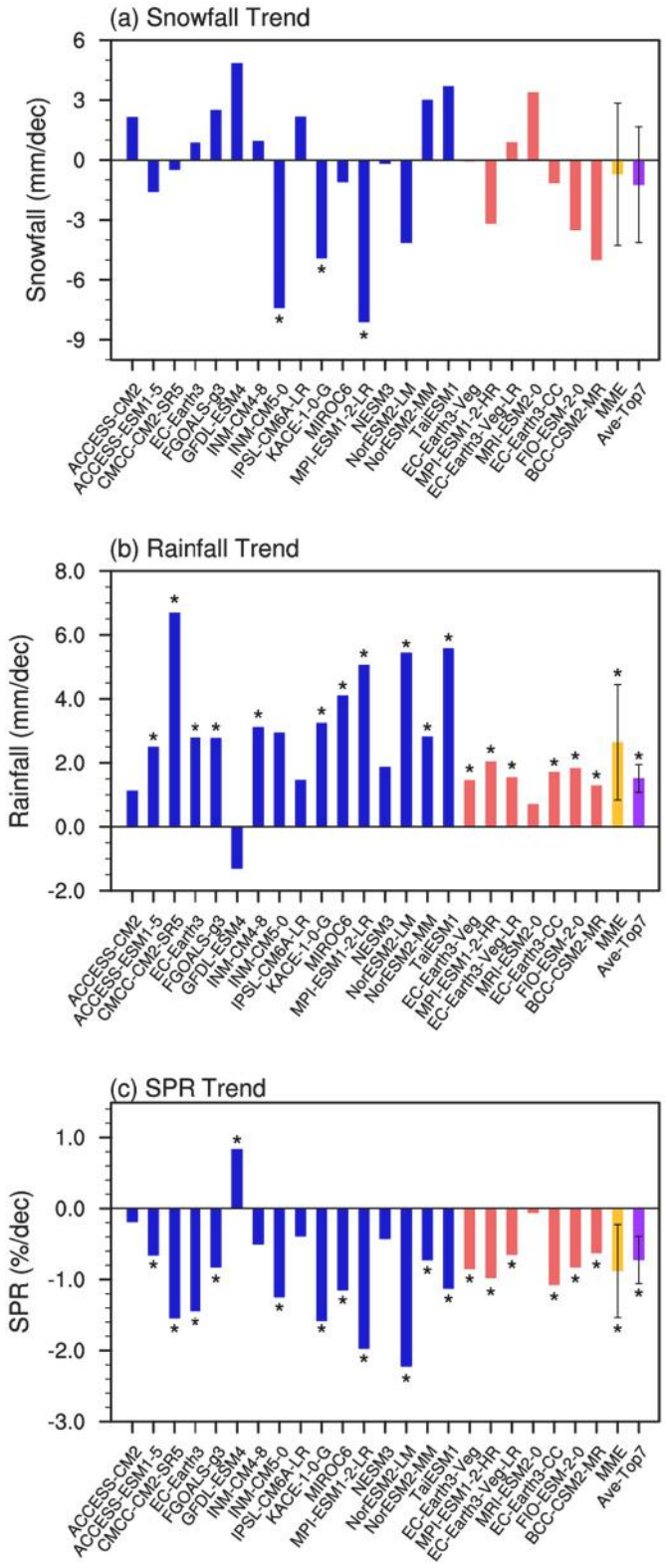

Fig. 7. Trend of cold-season average (a) snowfall, (b) rainfall and (c) SPR over the TP during the 1979–2017 period. The red bars represent the seven best models for SPR simulation, the blue bars represent other models, the yellow bar represents CMIP6 MME, and the purple bar represents MME of the seven best models. The error bar denotes the two standard deviations of simulations. Bars with * represent statistically significant trends ($p < 0.05$). (For interpretation of the references to colour in this figure legend, the reader is referred to the web version of this article.)

>20%, which means that more snowfall would transition to rainfall and reduce the recharge of the Asian water tower. Although the result is more reliable than 23 CMIP6 MME, it should be noted that the project of the top seven CMIP6 models still has great uncertainties, which need extra caution when quoting the aforementioned result.

4. Conclusion and discussion

Due to the scarcity of observations, simulations are an important tool to investigate climate changes over the TP. However, the simulations remain large uncertainties due to the complex terrain and coarse resolution in the models. Reliable precipitation phase simulation is the key to studying the mechanism of the imbalance of the Asian water tower (Yao et al., 2022) and predicting the availability of future water resources (Flato et al., 2013). Our research evaluates the performance of 23 CMIP6 models for the precipitation phase in the cold season over the TP. The precipitation phase was represented by the snowfall-precipitation-ratio (SPR). The results found that the climatology of SPR is underestimated and the decreasing trend of SPR is overestimated in the CMIP6 MME compared with the CMFD. However, there are significant differences in the simulated SPR by different CMIP6 models. Among these models, the relationship between SPR bias and thermal factors (temperature bias) and dynamic factors (total precipitation bias) were further investigated. The results found that the SPR bias in the cold season over the TP is sensitive to temperature bias and is less sensitive to total precipitation bias. One of the reasons is that the enhanced warming during the cold season will increase the melting level height (MLH), causing a transition from snowfall to rainfall over the TP (Prein and Heymsfield, 2020; Wang et al., 2022). Once the ambient wet-bulb temperature (or ice bulb temperature) reaches 0 °C, the ice particles will begin to melt (Wilson, 1941; Prein and Heymsfield, 2020). Consequently, the vertical height of the zero-degree wet-bulb temperature above the surface (also known as the melting level height) has a significant impact on the type of precipitation. Previous studies have demonstrated that the MLH is mainly affected by the surface temperature; as a key factor, the MLH establishes a physical link between the surface temperature and the melting of ice particles when they fall into the troposphere (Wang et al., 2021). During model simulations, the surface temperature bias will influence the precipitation phase bias through the MLH during the cold season. In CMIP6 models, for instance, the higher the surface temperature is, the lower the simulated SPR. The high correlation between the SPR- trend and the temperature- trend in the cold season also demonstrates that the performance of CMIP6 models in simulating cold-season temperature is the key to accurately simulating the precipitation phase in the cold season over the TP.

When ranked based on spatial and temporal climate features of SPR, the top seven models (EC-Earth3-Veg, MPI-ESM1–2-HR, EC-Earth3-Veg-LR, MRI-ESM2–0, EC-Earth3-CC, FIO-ESM-2-0, BCC-CSM2-MR) with good performance in historical simulation are selected. The top seven best models show a significant decreasing trend of SPR under the SSP245 and SSP585 scenarios. The SPR in the cold season over the TP will decrease by approximately 2.93–3.38% in the near term, 5.13–7.2% in the midterm and 9.79–21.45% in the long term. However, the long-term decline in SPR will not exceed 2% according to the observational trend in recent decades. The result suggests that the precipitation phase represented by SPR will rapidly transition from snowfall to rainfall, especially under the SSP585 scenario, and that the cold-season SPR over the TP will decrease with an alarming trend. Since liquid precipitation is more likely to be lost than solid precipitation, the change poses a great threat to local water security. However, it must be noted that even for models with good performance of historical SPR, their projection in the future always has substantial uncertainty. Emergent constraint is an effective method to reduce the uncertainty of model projections (Lian et al., 2018; Hall et al., 2019; Tokarska et al., 2020) and is recommended to further verify the projection and reduce the uncertainty. The above research and new views will help the development of climate models.

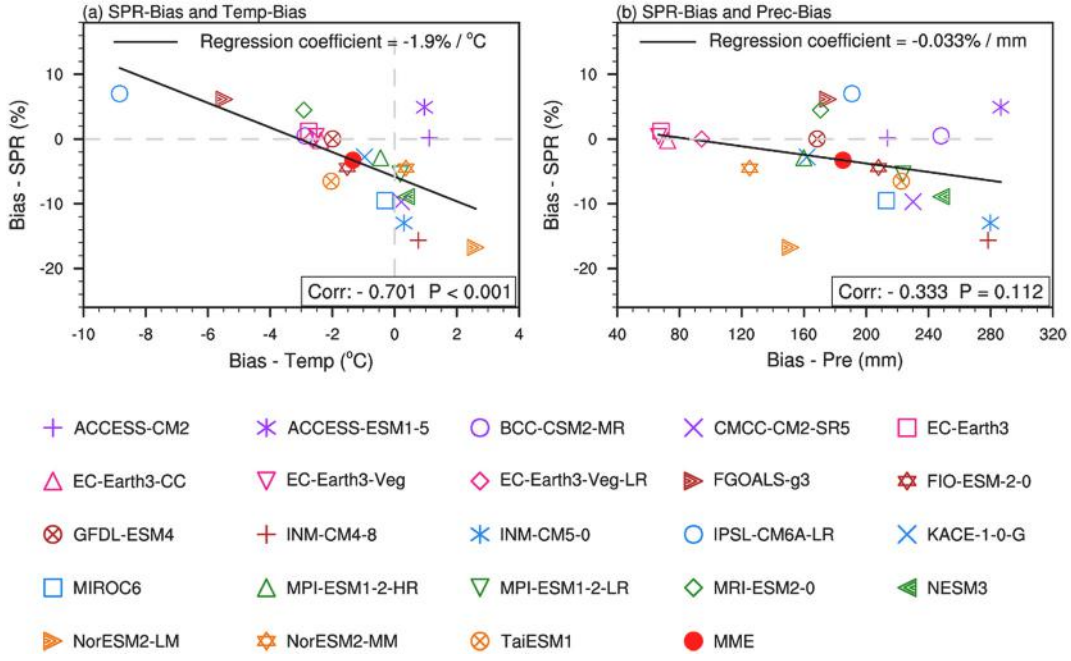

Fig. 8. The scatter distribution of 23 CMIP6 model-simulated (a) temperature bias and (b) precipitation bias with SPR bias in the cold season over the TP. The black line indicates their regression relationship.

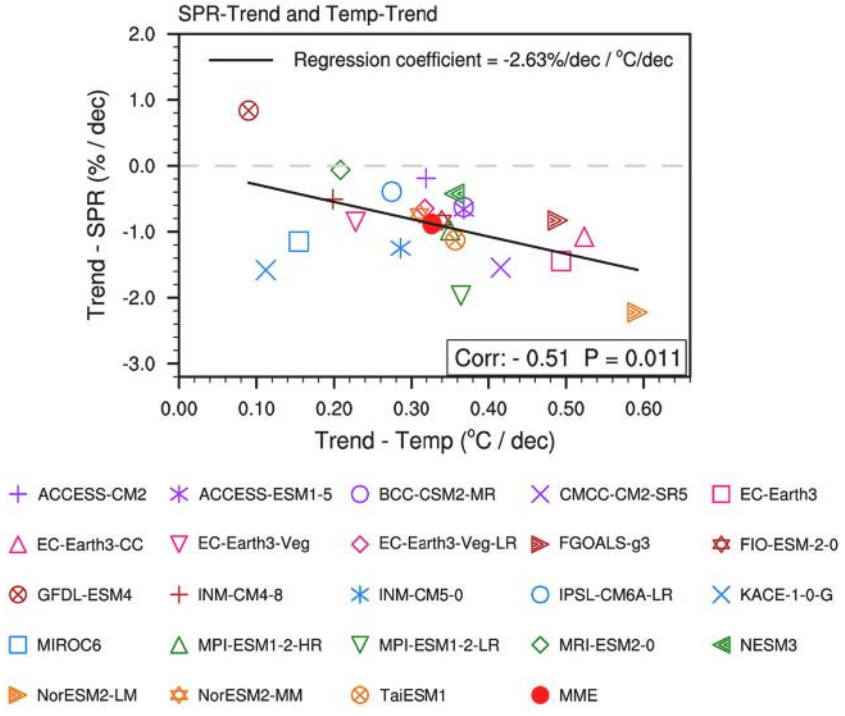

Fig. 9. The scatter distribution of 23 CMIP6 models simulated the warming trend with the SPR trend in the cold season over the TP. The black line indicates their regression relationship.

Recommended models from CMIP6 in this study could provide a scientific reference for future climate change projections over the TP.

CRediT authorship contribution statement

Guodong Wang: Methodology, Software, Writing – original draft, Visualization. **Yongli He:** Conceptualization, Methodology, Writing – review & editing, Supervision, Funding acquisition. **Boyuan Zhang:** Software, Validation, Writing – review & editing. **Xiaoxia Wang:** Writing – review & editing. **Shanjun Cheng:** Writing – review & editing. **Yongkun Xie:** Writing – review & editing. **Shanshan Wang:** Writing – review & editing. **Xiaodan Guan:** Writing – review & editing.

Declaration of Competing Interest

The authors declare that they have no known competing financial

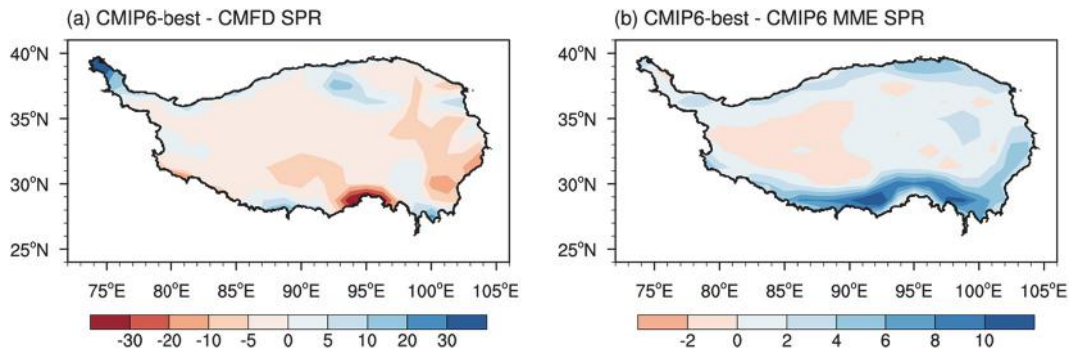

Fig. 10. (a) The spatial difference of the cold-season average SPR between the MME of the selected seven best models and CMFD during 1979–2017. (b) The spatial difference in the cold-season average SPR between the MME of the selected seven best models and the MME of 23 CMIP6 models during 1979–2017.

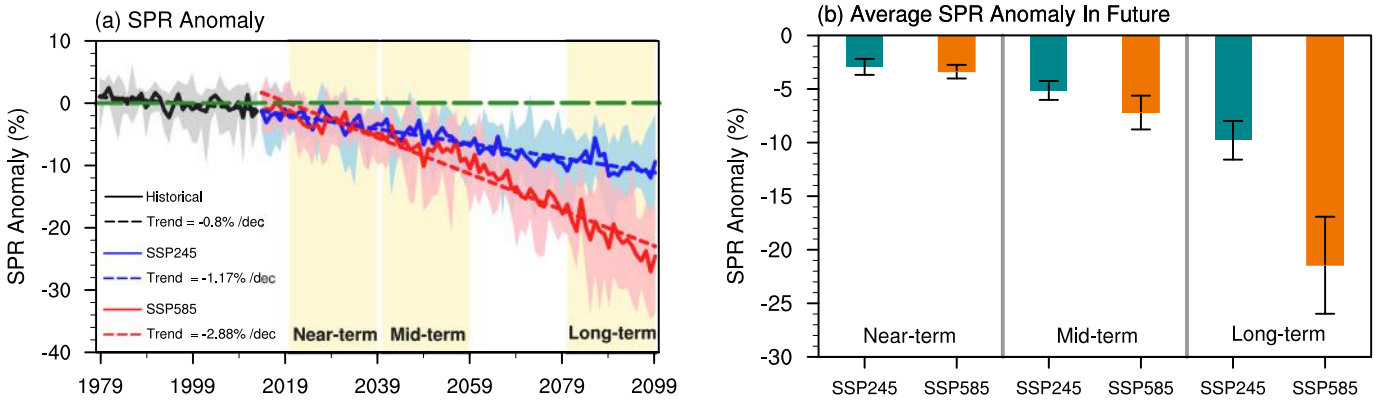

Fig. 11. (a) Time series of cold-season SPR anomalies (relative to 1979–2013) over the TP during 1979–2099 from the seven best CMIP6 models. The lines show the means of the seven best models in the historical (black), SSP245 (blue), and SSP585 (red) scenarios. Shading denotes the maximum and minimum values of the seven best models. (b) The cold-season SPR changes (relative to 1979–2013) under the SSP245 (green) and SSP585 (orange) scenarios over the TP in the near-term (2020–2039), mid-term (2040–2059) and long-term (2080–2099) future. Projections are derived from the means of the seven best models. The error bar denotes two standard deviations of the seven best models, which reflects the 95% confidence interval. (For interpretation of the references to colour in this figure legend, the reader is referred to the web version of this article.)

interests or personal relationships that could have appeared to influence the work reported in this paper.

Data availability

Data will be made available on request.

Acknowledgment

This work was jointly supported by the Strategic Priority Research Program of the Chinese Academy of Sciences (XDA2006010301), the National Science Foundation of China (42041004 and 91837209), the National Key Research and Development Program of China (No. 2019YFA0607104), the China 111 Project (B13045) and the Fundamental Research Funds for the Central Universities (lzujbky-2021-sp07). The Supercomputing Center of Lanzhou University also supported this work. The CMIP6 data can be accessed through https://esgf-node.llnl.gov/search/cmip6/. The CMFD are available from https://esgf-node.llnl.gov/search/cmip6/, and the IMERG datasets are available from https://disc.gsfc.nasa.gov/.

Appendix A. Supplementary data

Supplementary data to this article can be found online at https://doi.org/10.1016/j.atmosres.2022.106494.

References

Allen, M.R., Ingram, W.J., 2002. Constraints on future changes in climate and the hydrologic cycle. Nature. 419 (6903), 228–232. https://doi.org/10.1038/nature01092.

Bocchieri, J.R., 1980. The objective use of upper air soundings to specify precipitation type. Mon. Weather Rev. 108 (5), 596–603. https://doi.org/10.1175/1520-0493(1980)108<0596:TOUOUA>2.0.CO;2.

Chen, L., Frauenfeld, O.W., 2014. A comprehensive evaluation of precipitation simulations over China based on CMIP5 multimodel ensemble projections. J. Geophys. Res. Atmos. 119 (10), 5767–5786. https://doi.org/10.1002/2013JD021190.

Chen, D., Xu, B., Yao, T., Guo, Z., Cui, P., Chen, F., et al., 2015. Assessment of past, present and future environmental changes on the Tibetan Plateau. Chin. Sci. Bull. 60 (32), 3025–3035. https://doi.org/10.1360/N972014-01370.

Chen, X., Liu, Y., Wu, G., 2017. Understanding the surface temperature cold bias in CMIP5 AGCMs over the Tibetan Plateau. Adv. Atmos. Sci. 34 (12), 1447–1460. https://doi.org/10.1007/s00376-017-6326-9.

Deng, H., Pepin, N.C., Chen, Y., 2017. Changes of snowfall under warming in the Tibetan Plateau. J. Geophys. Res. Atmos. 122 (14), 7323–7341. https://doi.org/10.1002/2017JD026524.

Ding, B., Yang, K., Qin, J., Wang, L., Chen, Y., He, X., 2014. The dependence of precipitation types on surface elevation and meteorological conditions and its parameterization. J. Hydrol. 513, 154–163. https://doi.org/10.1016/j.jhydrol.2014.03.038.

Duan, A., Xiao, Z., 2015. Does the climate warming hiatus exist over the Tibetan Plateau? Sci. Rep. 5, 13711. https://doi.org/10.1038/srep13711.

Duan, Z., Liu, J., Tuo, Y., Chiogna, G., Disse, M., 2016. Evaluation of eight high spatial resolution gridded precipitation products in Adige Basin (Italy) at multiple temporal and spatial scales. Sci. Total Environ. 573, 1536–1553. https://doi.org/10.1016/j.scitotenv.2016.08.213.

Eyring, V., Bony, S., Meehl, G.A., Senior, C.A., Stevens, B., Stouffer, R.J., Taylor, K.E., 2016. Overview of the coupled model intercomparison project phase 6 (CMIP6) experimental design and organization. Geosci. Model Dev. 9 (5), 1937–1958. https://doi.org/10.5194/gmd-9-1937-2016.

Flato, G., Marotzke, J., Abiodun, B., Braconnot, P., Chou, S.C., Collins, W., Rummukainen, M., 2013. Evaluation of climate models. In: Stocker, T.F., et al. (Eds.), Climate Change 2013: The Physical Science Basis. Contribution of Working Group I to the Fifth Assessment Report of the Intergovernmental Panel on Climate Change. Cambridge University Press, Cambridge, UK, and New York, pp. 741–882.

Gidden, M.J., Riahi, K., Smith, S.J., Fujimori, S., Luderer, G., Kriegler, E., et al., 2019. Global emissions pathways under different socioeconomic scenarios for use in CMIP6: a dataset of harmonized emissions trajectories through the end of the century. Geosci. Model Dev. 12 (4), 1443–1475. https://doi.org/10.5194/gmd-2018-266.

Gilleland, E., 2020. Bootstrap methods for statistical inference. Part I: comparative forecast verification for continuous variables. J. Atmos. Ocean. Technol. 37 (11), 2117–2134. https://doi.org/10.1175/JTECH-D-20-0069.1.

Hall, A., Cox, P., Huntingford, C., Klein, S., 2019. Progressing emergent constraints on future climate change. Nat. Clim. Chang. 9 (4), 269–278. https://doi.org/10.1038/s41558-019-0436-6.

He, J., Yang, K., Tang, W., Lu, H., Qin, J., Chen, Y., Li, X., 2020. The first high-resolution meteorological forcing dataset for land process studies over China. Sci. Data. 7 (1), 1–11. https://doi.org/10.1038/s41597-020-0369-y.

He, Y., Tian, W., Huang, J., Wang, G., Ren, Y., Yan, H., et al., 2021. The mechanism of increasing summer water vapor over the Tibetan Plateau. J. Geophys. Res. Atmos. 126 (10), 1–18. https://doi.org/10.1029/2020JD034166.

Hou, A.Y., Kakar, R.K., Neeck, S., Azarbarzin, A.A., Kummerow, C.D., Kojima, M., et al., 2014. The global precipitation measurement mission. Bull. Am. Meteorol. Soc. 95 (5), 701–722. https://doi.org/10.1175/BAMS-D-13-00164.1.

Huang, J., Chen, W., Wen, Z., Zhang, G., Li, Z., Zuo, Z., Zhao, Q., 2019. Review of Chinese atmospheric science research over the past 70 years: climate and climate change. Sci. China Earth Sci. 62 (10), 1514–1550. https://doi.org/10.1007/s11430-019-9483-5.

Huffman, G.J., Stocker, E.F., Bolvin, D.T., Nelkin, E.J., Tan, Jackson, 2019. GPM IMERG Final Precipitation L3 Half Hourly 0.1 degree x 0.1 degree V06. In: Greenbelt, MD, Goddard Earth Sciences Data and Information Services Center (GES DISC). https://doi.org/10.5067/GPM/IMERG/3B-HH/06.

Immerzeel, W.W., Bierkens, M.F.P., 2012. Asia's water balance. Nat. Geosci. 5 (12), 841–842. https://doi.org/10.1038/ngeo1643.

Immerzeel, W.W., Van Beek, L.P., Bierkens, M.F., 2010. Climate change will affect the Asian water towers. Science. 328 (5984), 1382–1385. https://doi.org/10.1126/science.1183188.

Jia, K., Ruan, Y., Yang, Y., You, Z., 2019. Assessment of CMIP5 GCM simulation performance for temperature projection in the Tibetan Plateau. Earth Space Sci. 6 (12), 2362–2378. https://doi.org/10.1029/2019EA000962.

Kang, S., Xu, Y., You, Q., Flügel, W.A., Pepin, N., Yao, T., 2010. Review of climate and cryospheric change in the Tibetan Plateau. Environ. Res. Lett. 5 (1), 015101 https://doi.org/10.1088/1748-9326/5/1/015101.

Kuang, X., Jiao, J.J., 2016. Review on climate change on the Tibetan Plateau during the last half century. J. Geophys. Res. Atmos. 121 (8), 3979–4007. https://doi.org/10.1002/2015JD024728.

Li, Q., Wei, J., Yin, J., Qiao, Z., Peng, W., Peng, H., 2020. Multiscale comparative evaluation of the GPM and TRMM precipitation products against ground precipitation observations over Chinese Tibetan Plateau. IEEE J. Sel. Topics Appl. Earth Observ. Remote Sens. 14, 2295–2313. https://doi.org/10.1109/JSTARS.2020.3047897.

Li, Y., Wang, C., Su, F., 2021. Evaluation of CMIP6 models over two third pole subregions with contrasting circulation systems. J. Clim. 34 (22), 9133–9152. https://doi.org/10.1175/JCLI-D-21-0214.1.

Li, D., Qi, Y., Chen, D., 2022. Changes in rain and snow over the Tibetan Plateau based on IMERG and Ground-based observation. J. Hydrol. 606, 127400 https://doi.org/10.1016/j.jhydrol.2021.127400.

Lian, X., Piao, S., Huntingford, C., Li, Y., Zeng, Z., Wang, X., et al., 2018. Partitioning global land evapotranspiration using CMIP5 models constrained by observations. Nat. Clim. Chang. 8 (7), 640–646. https://doi.org/10.1038/s41558-018-0207-9.

Lu, C., Yu, G., Xie, G., 2005. Tibetan plateau serves as a water tower. Int. Geosci. Remote Sens. Symp. (IGARSS) 5, 3120–3123. https://doi.org/10.1109/IGARSS.2005.1526498.

Lun, Y., Liu, L., Cheng, L., Li, X., Li, H., Xu, Z., 2021. Assessment of GCMs simulation performance for precipitation and temperature from CMIP5 to CMIP6 over the Tibetan Plateau. Int. J. Climatol. 41 (7), 3994–4018. https://doi.org/10.1002/joc.7055.

Luo, J., Chen, H., Zhou, B., 2020. Comparison of snowfall variations over china identified from different snowfall/rainfall discrimination methods. J. Meteorol. Res. 34, 1114–1128. https://doi.org/10.1007/s13351-020-0004-z.

McCrystall, M.R., Stroeve, J., Serreze, M., Forbes, B.C., Screen, J.A., 2021. New climate models reveal faster and larger increases in Arctic precipitation than previously projected. Nat. Commun. 12 (1), 1–12. https://doi.org/10.1038/s41467-021-27031-y.

Meng, F., Su, F., Li, Y., Tong, K., 2019. Changes in terrestrial water storage during 2003–2014 and possible causes in Tibetan Plateau. J. Geophys. Res. Atmos. 124 (6), 2909–2931. https://doi.org/10.1029/2018JD029552.

Nury, A.H., Sharma, A., Marshall, L., Mehrotra, R., 2019. Characterising uncertainty in precipitation downscaling using a Bayesian approach. Adv. Water Resour. 129, 189–197. https://doi.org/10.1016/j.advwatres.2019.05.018.

O'Neill, B.C., Tebaldi, C., Van Vuuren, D.P., Eyring, V., Friedlingstein, P., Hurtt, G., et al., 2016. The scenario model intercomparison project (ScenarioMIP) for CMIP6. Geosci. Model Dev. 9 (9), 3461–3482. https://doi.org/10.5194/gmd-9-3461-2016.

Palazzi, E., von Hardenberg, J., Terzago, S., Provenzale, A., 2015. Precipitation in the Karakoram-Himalaya: a CMIP5 view. Clim. Dyn. 45 (1), 21–45. https://doi.org/10.1007/s00382-014-2341-z.

Peng, Y., Duan, A., Hu, W., Tang, B., Li, X., Yang, X., 2022. Observational constraint on the future projection of temperature in winter over the Tibetan Plateau in CMIP6 models. Environ. Res. Lett. 17 (3) https://doi.org/10.1088/1748-9326/ac541c.

Prein, A.F., Heymsfield, A.J., 2020. Increased melting level height impacts surface precipitation phase and intensity. Nat. Clim. Chang. 10 (8), 771–776. https://doi.org/10.1038/s41558-020-0825-x.

Rangwala, I., Miller, J.R., Xu, M., 2009. Warming in the Tibetan Plateau: possible influences of the changes in surface water vapor. Geophys. Res. Lett. 36 (6), 1–6. https://doi.org/10.1029/2009GL037245.

Rivera, J.A., Arnould, G., 2020. Evaluation of the ability of CMIP6 models to simulate precipitation over Southwestern South America: Climatic features and long-term trends (1901–2014). Atmos. Res. 241, 104953 https://doi.org/10.1016/j.atmosres.2020.104953.

Scherrer, S.C., 2011. Present-day interannual variability of surface climate in CMIP3 models and its relation to future warming. Int. J. Climatol. 31 (10), 1518–1529. https://doi.org/10.1002/joc.2170.

Shiferaw, A., Tadesse, T., Rowe, C., Oglesby, R., 2018. Precipitation extremes in dynamically downscaled climate scenarios over the Greater Horn of Africa. Atmosphere. 9 (3), 112. https://doi.org/10.3390/atmos9030112.

Su, F., Duan, X., Chen, D., Hao, Z., Cuo, L., 2013. Evaluation of the global climate models in the CMIP5 over the Tibetan Plateau. J. Clim. 26 (10), 3187–3208. https://doi.org/10.1175/JCLI-D-12-00321.1.

Sun, J., Yang, K., Guo, W., Wang, Y., He, J., Lu, H., 2020. Why has the inner Tibetan Plateau become wetter since the mid-1990s? J. Clim. 33 (19), 8507–8522. https://doi.org/10.1175/JCLI-D-19-0471.1.

Tamang, S.K., Ebtehaj, A.M., Prein, A.F., Heymsfield, A.J., 2020. Linking global changes of snowfall and wet-bulb temperature. J. Clim. 33 (1), 39–59. https://doi.org/10.1175/JCLI-D-19-0254.1.

Tokarska, K.B., Stolpe, M.B., Sippel, S., Fischer, E.M., Smith, C.J., Lehner, F., Knutti, R., 2020. Past warming trend constrains future warming in CMIP6 models. Sci. Adv. 6 (12), eaaz9549. https://doi.org/10.1126/sciadv.aaz9549.

Tropea, B., Stewart, R., 2021. Assessing past and future hazardous freezing rain and wet snow events in Manitoba, Canada using a pseudo-global warming approach. Atmos. Res. 259, 105656 https://doi.org/10.1016/j.atmosres.2021.105656.

Wang, J., Zhang, M., Wang, S., Ren, Z., Che, Y., Qiang, F., Qu, D., 2016. Decrease in snowfall/rainfall ratio in the Tibetan Plateau from 1961 to 2013. J. Geogr. Sci. 26 (9), 1277–1288. https://doi.org/10.1007/s11442-016-1326-8.

Wang, Y., Yang, K., Zhou, X., Chen, D., Lu, H., Ouyang, L., et al., 2020. Synergy of orographic drag parameterization and high resolution greatly reduces biases of WRF-simulated precipitation in central Himalaya. Clim. Dyn. 54 (3–4), 1729–1740. https://doi.org/10.1007/s00382-019-05080-w.

Wang, J., Guan, Y., Wu, L., Guan, X., Cai, W., Huang, J., et al., 2021. Changing lengths of the four seasons by global warming. Geophys. Res. Lett. 48 (6) https://doi.org/10.1029/2020GL091753.

Wang, G., He, Y., Huang, J., Guan, X., Wang, X., Hu, H., et al., 2022. The influence of precipitation phase changes on the recharge process of terrestrial water storage in the cold season over the Tibetan Plateau. J. Geophys. Res. Atmos. 127 https://doi.org/10.1029/2021JD035824.

Wilson, W.T., 1941. An outline of the thermodynamics of snow-melt. Eos Trans. AGU 22 (1), 182–195. https://doi.org/10.1029/TR022i001p00182.

Xu, X., Lu, C., Shi, X., Gao, S., 2008. World water tower: an atmospheric perspective. Geophys. Res. Lett. 35 (20), 1–5. https://doi.org/10.1029/2008GL035867.

Xu, X., Zhao, T., Lu, C., Guo, Y., Chen, B., Liu, R., et al., 2014. An important mechanism sustaining the atmospheric water tower over the Tibetan Plateau. Atmos. Chem. Phys. Discuss. 14 (12), 18255–18275. https://doi.org/10.5194/acpd-14-18255-2014.

Yang, K., He, J., 2019. China meteorological forcing dataset (1979–2018). National Tibetan Plateau Data Center 670. https://doi.org/10.11888/AtmosphericPhysics.tpe.249369.file.

Yang, X., Zhou, B., Xu, Y., Han, Z., 2021. CMIP6 evaluation and projection of temperature and precipitation over China. Adv. Atmos. Sci. 38 (5), 817–830. https://doi.org/10.1007/s00376-021-0351-4.

Yao, T., Thompson, L., Yang, W., Yu, W., Gao, Y., Guo, X., et al., 2012. Different glacier status with atmospheric circulations in Tibetan Plateau and surroundings. Nat. Clim. Chang. 2 (9), 663–667. https://doi.org/10.1038/nclimate1580.

Yao, T., Xue, Y., Chen, D., Chen, F., Thompson, L., Cui, P., et al., 2019. Recent third pole's rapid warming accompanies cryospheric melt and water cycle intensification and interactions between monsoon and environment: Multidisciplinary approach with observations, modeling, and analysis. Bull. Amer. Meteor. Soc. 100 (3), 423–444. https://doi.org/10.1175/BAMS-D-17-0057.1.

Yao, T., Bolch, T., Chen, D., Gao, J., Immerzeel, W., Piao, S., et al., 2022. The imbalance of the Asian water tower. Nat. Rev. Earth Environ. 1-15 https://doi.org/10.1038/s43017-022-00299-4.

Yazdandoost, F., Moradian, S., Izadi, A., Aghakouchak, A., 2021. Evaluation of CMIP6 precipitation simulations across different climatic zones: uncertainty and model intercomparison. Atmos. Res. 250, 105369 https://doi.org/10.1016/j.atmosres.2020.105369.

Zhao, Y., Zhou, T., Zhang, W., Li, J., 2022. Change in precipitation over the Tibetan Plateau projected by weighted CMIP6 models. Adv. Atmos. Sci. 39 (7), 1133–1150. https://doi.org/10.1007/s00376-022-1401-2.

Zhu, K., Guan, X., Huang, J., Wang, J., Guo, S., Cao, C., 2021. Precipitation over semi-arid regions of North Hemisphere affected by Atlantic Multidecadal Oscillation. Atmos. Res. 262, 105801 https://doi.org/10.1016/j.atmosres.2021.105801.